J Mater Sci (2010) 45:3727–3734
DOI 10.1007/s10853-010-4421-8

Microstructure and mechanical properties of Al-base composites by addition of Al–Ni–Co decagonal quasicrystalline particles through a mechanical stirring route

Man Zhu · Gencang Yang · Lijuan Yao · Suling Cheng · Yaohe Zhou

Received: 6 November 2009 / Accepted: 16 March 2010 / Published online: 27 March 2010

Abstract In the present study, the A356Al-base composite materials were fabricated by introducing 2.5, 5, 7.5, 10 mass% of Al–Ni–Co decagonal quasicrystalline particles using the mechanical stirring method. The microstructures, mechanical properties, and Brinell hardness of these composites were investigated in detail by means of scanning electron microscopy (SEM) and energy dispersive spectroscopy (EDS). It is found that serious compositional diffusion occurs between the $Al_{72}Ni_{12}Co_{16}$ quasicrystalline particles and the Al melt. Microstructural analysis of all as-cast composites shows that the structure of the quasicrystal disappears and is replaced by the formation of two crystalline phases, Co-rich θ-phase and Ni-rich γ-phase which all contain Al, Si, Ni, and Co. The particle sizes of the two crystalline phases are much smaller than that of the original decagonal quasicrystalline phase. The composites exhibit improvement of 10.5–24% and 20–25% in yield strength and Brinell hardness, respectively, while the percent elongation decreases obviously. Examination of the fracture surface of the as-cast A356Al-base composites shows that they exhibit typical brittle fracture mode.

M. Zhu
School of Materials and Chemical Engineering,
Xi'an Technological University, Xi'an, Shaanxi 710032,
People's Republic of China

M. Zhu (✉) · G. Yang · S. Cheng · Y. Zhou
State Key Laboratory of Solidification Processing, Northwestern Polytechnical University, Xi'an, Shaanxi 710072,
People's Republic of China
e-mail: zm0428@mail.nwpu.edu.cn

L. Yao
Foundry Technology, Xi'an, Shaanxi 710005,
People's Republic of China

Introduction

A composite material is a combination of two or more distinct material phases. Metal matrix composites (MMCs), especially Al-metal matrix composites, have emerged as an advanced engineering materials in the field of aerospace and automotive industries due to their high strength and stiffness, excellent elastic modulus, good thermal and mechanical fatigue, and creep resistance than those of monolithic materials [1, 2]. Nowadays, particulate reinforced metal matrix composites (PRMMCs) are one of the most popular composites and receive wide application, because they provide essentially isotropic properties and reasonable ductility. The most commonly developed PRMMCs are Al-base composites with SiC and/or Al_2O_3 reinforcing particles [1, 3–5]. However, the complex fabrication process and high production cost of current PRMMCs, such as Al/SiC_p MMCs, are still strong barriers which hinder their extensive application. Thus, the research on the development of low-cost PRMMCs with high properties is still needed.

Following the first discovery of icosahedral quasicrystals by Schetman et al. [6], extensive theoretical and experimental studies on Al-base composites reinforced by quasicrystals have been carried out, because quasicrystals (QC) have the advantages of brittleness, hardness, low frictional coefficient, and good wear-resistance. In 1993, Al-base composites using Al powder and $Al_{64}Cu_{24}Fe_{12}$ icosahedral quasicrystal powder were fabricated successfully by Tsai et al. [7]. In these composites, the hardness was improved remarkably and reached the maximum value of 120 kg/mm^2 for a 25 vol.% $Al_{64}Cu_{24}Fe_{12}$ particle reinforcement content. Al-base composites reinforced by quasicrystalline particles were also studied by many researchers using powder metallurgy [8–13], where the

icosahedral quasicrystalline alloys, i.e., Al–Cu–Fe and Al–Cu–Cr, were always selected as the reinforcing phase.

Following the $Al_{100-2x}Ni_xCo_x$ pseudo binary phase diagram established by Yokoyama et al. [14], Al–Ni–Co single-phase quasicrystal, with a chemical composition in the vicinity of $Al_{72}Ni_{12}Co_{16}$ (at.%), was prepared using the Czochralski method. The fabrication process, microstructural characterization, and growth behavior in $Al_{72}Ni_{12}Co_{16}$ decagonal quasicrystal (D-AlNiCo) were investigated in detail, and it was found that it showed high thermodynamic stability [15–18]. Unlike icosahedral quasicrystal, the decagonal quasicrystal possesses both quasiperiodic and periodic directions in one grain. However, Al-base composites reinforced by single-phase decagonal quasicrystals were rarely reported. In order to explore and develop the application areas of quasicrystalline materials, we investigated the use of A356 foundry aluminum alloy and $Al_{72}Ni_{12}Co_{16}$ decagonal quasicrystalline particles to prepare PRMMCs. The stability of $Al_{72}Ni_{12}Co_{16}$ decagonal quasicrystal in the Al melt was studied. The microstructures, mechanical properties, and strengthening mechanisms of the A356Al-base composites were also investigated.

Experimental

Materials

The materials used in the present study are commercial A356 alloy and D-AlNiCo particles. The chemical composition of A356 alloy is 6.92Si–0.29 Mg–0.18Ti–0.099Fe–0.0071Cu-bal Al (in weight percent). The $Al_{72}Ni_{12}Co_{16}$ quasicrystalline alloy was prepared by melting pure Al, Ni, and Co (purity ≥99.8 wt%) in a medium frequency induction furnace, and the melt was poured into a graphite mold. ICP-AES examination revealed that the composition of the above quasicrystalline alloy fits well with the nominal composition. The quasicrystalline alloy was mechanically crushed into several millimeters in size, following which D-AlNiCo particles were obtained by ball milling and sieving. Sieve sizes of D-AlNiCo particles, ranging from 53 to 147 μm, were preserved for use. The D-AlNiCo particles were cleaned 5–7 times using acetone in order to remove the fine particles attached to the big ones.

Experimental procedure

The A356 aluminum alloy was used as a matrix, and the D-AlNiCo particles were selected as the reinforcing phase. The A356Al-base composites were fabricated by mechanical stirring method. The schematic diagram of the experimental apparatus is given in Fig. 1. The main equipment is as follows: furnace, graphite crucible, a motor, stirring equipment, and K-type thermocouple. The particles are introduced into the Al melt through the funnel. The stirring speed of the melt can be controlled by using the adjustable speed motor. The K-type thermocouple is used to measure the temperature of the melt.

First, the A356 alloy was melted using an electric resistance furnace. The melt was refined using hexachloroethane and then degassed by pure Ar at 730 °C. Subsequently, the melt temperature was lowered below the

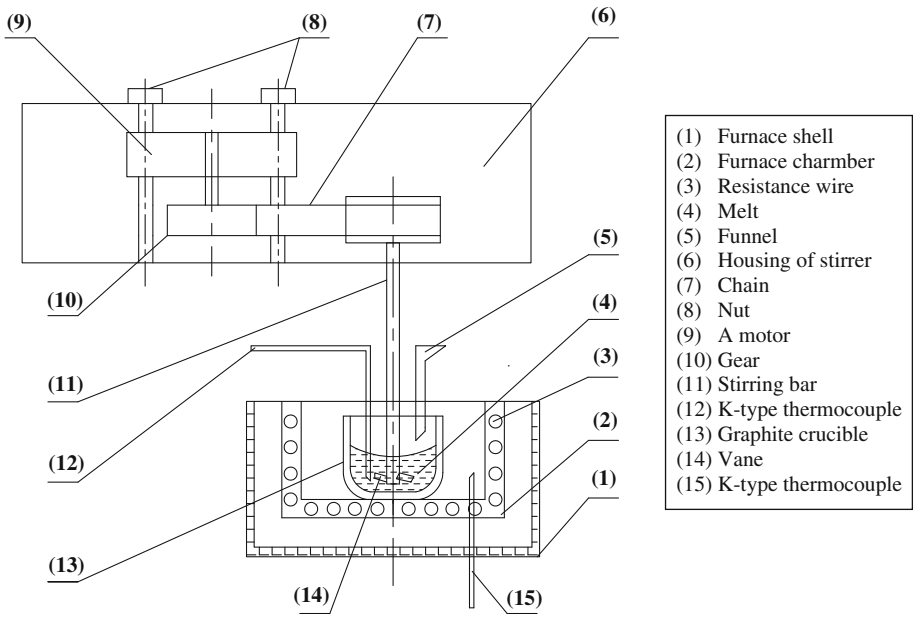

Fig. 1 The schematic diagram of the experimental set-up apparatus

liquidus, to the semi-solid state. When it reached 610 °C, the D-AlNiCo particles, preheated at 500 °C for 2 h, were added into the slurry and stirred continuously for 10 min to disperse the particles uniformly. The addition level of the D-AlNiCo particles ranged from 2.5 to 10 wt% in steps of 2.5%. After that, the composite slurry was reheated to 720 °C and stirred again for 5 min. Finally, the melt was poured into a preheated metal mould (at about 300 °C). The fabricated composites were of a size 18 mm in diameter and 130 mm in height.

Characterization and tests

After cashing the composites, specimens for metallography were cut from the castings and mechanically polished. The microstructures were characterized by means of optical microscopy (OM; Olympus PMG) and scanning electron microscopy (SEM; Tescan VegaII). The local phase compositions were determined using energy dispersive spectroscopy (EDS; Oxford Inca 350). The tensile tests were performed using a universal tensile testing machine (Instron 5581). The tested specimens were of cylindrical shape of 5 mm diameter and 25 mm gauge length. Each value of the tensile properties reported was the average value of four tensile specimens. After tensile tests, the tensile-fractured specimens were protected, cleaned, and cut along the tensile direction. The fracture surfaces of the tensile-tested samples were examined in a SEM under the secondary electron mode.

Results and discussion

Al–Ni–Co decagonal quasicrystal

Figure 2a shows the microstructure of the as-cast $Al_{72}Ni_{12}Co_{16}$ quasicrystalline alloy examined under backscatter electron (BSE) imaging mode, which shows that it contains a single phase, in addition to several small black voids representing casting defects. EDS qualitative analysis shows that the decagonal phase has an average composition of 71.55 at.% Al, 12.23 at.% Ni, and 16.22 at.% Co, which is quite consistent with the nominal composition of the as-prepared material. The XRD pattern further confirmed the existence of the single decagonal quasicrystalline phase (Fig. 2b).

After ball milling, the $Al_{72}Ni_{12}Co_{16}$ quasicrystalline alloy was broken into small particles, irregular polygon-like in shape with sharp edges, with clean surfaces and no finer particles attached to them, as is shown in Fig. 3. The washing of the particles with acetone using an ultrasonic wave washer ensured that the particles were of a high quality before adding them into the Al melt.

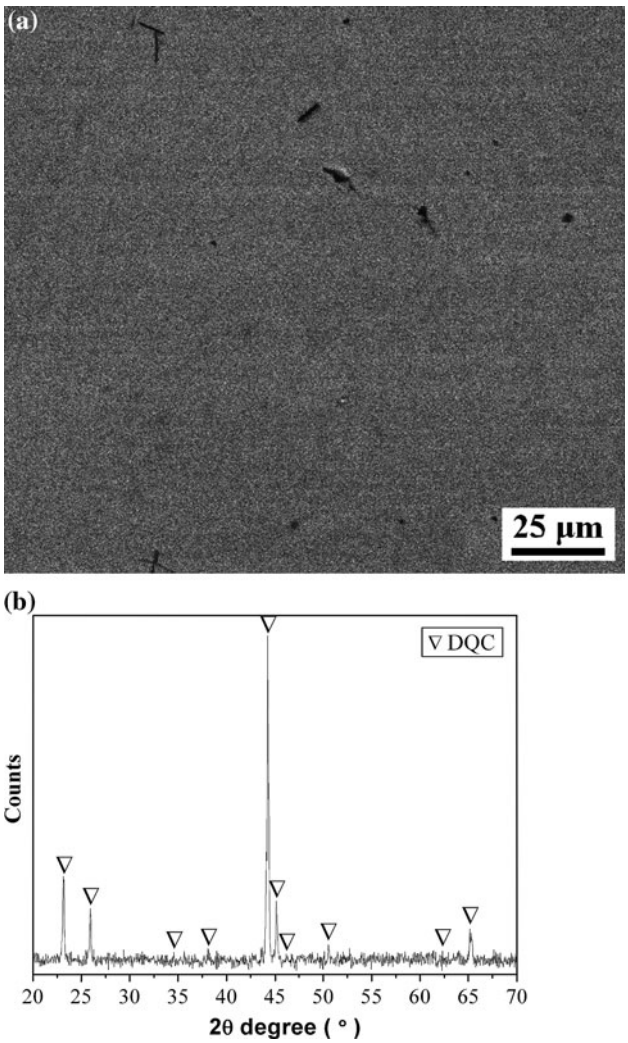

Fig. 2 BSE image (**a**) and XRD pattern (**b**) of the as-cast $Al_{72}Ni_{12}Co_{16}$ quasicrystalline alloy

Microstructures of the as-cast A356Al-base composites

Figure 4a–d shows the BSE images of A356Al-base composites containing different amounts of D-AlNiCo particles (2.5, 5.0, 7.5, and 10 wt%), where details in the microstructures may be observed clearly from the corresponding magnified images (Fig. 4e–h). The difference in contrast reflects the difference in composition. The BSE images in Fig. 4a–d show the microstructures of the A356Al-base composites consist of the α-Al matrix, eutectic silicon, and the white reinforcement particles. In the as-cast composites, the eutectic silicon, distributed randomly in the interdendritic regions has a coarse flake-like or acicular morphology, the same as that observed in A356 alloy. Non-uniform distribution of white reinforcement particles can be observed, distributed within the α-Al matrix and in the interdendritic regions.

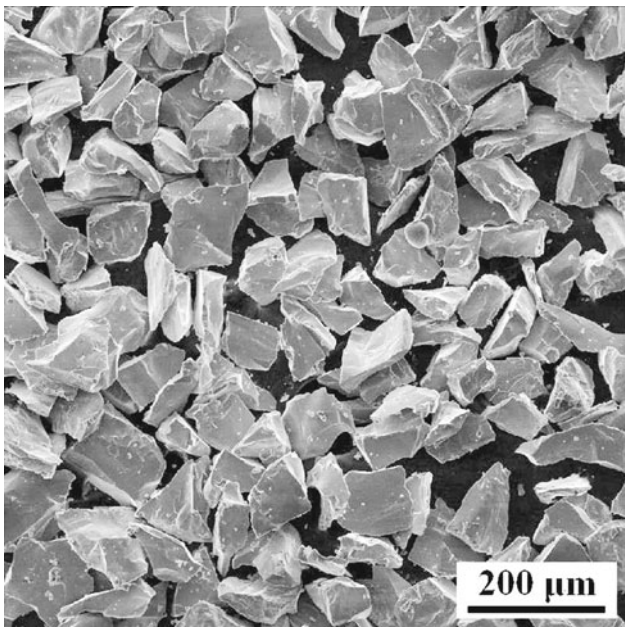

Fig. 3 The morphology of $Al_{72}Ni_{12}Co_{16}$ quasicrystalline particle after ball milling

The constitutional contrast shown in Fig. 4 does not distinguish clearly the white particles in α-Al matrix and the interdendritic regions. EDS analysis showed, however, that the white particles distributed in α-Al matrix and the interdendritic regions all contain Al, Si, Ni, and Co. The EDS results on the white particles in two regions are given in Table 1. The white particles distributed in α-Al matrix, named as θ-phase, contain 69.75–84.05 at.% Al, 1.21–1.93 at.% Si, 3.98–6.16 at.% Ni, and 9.41–14.03 at.% Co, whereas, the ones distributed in the interdendritic regions, named as γ-phase, have the average composition of 77.07–86.81 at.% Al, 0.80–3.84 at.% Si, 8.65–16.03 at.% Ni, and 0.71–4.37 at.% Co, as shown in Table 1. Based on the EDS results, for θ-phase and γ-phase, the contents of Al and Si are almost the same, while the contents of Ni and Co are different. Based on the Al–Ni and Al–Co binary phase diagrams [19], the maximum solute concentrations of Ni and Co in α-Al matrix are 0.023 and 0.009 at.%, respectively. EDS analysis shows that α-Al matrix contains 1.27 at.% Si, 0.01 at.% Ni, and 98.72 at.% Al, which means that just a small amount of Ni dissolves into the α-Al matrix; no Co is detected due to its extremely low solid solubility. The EDS results also revealed that no Ni and Co elements were detected in the eutectic silicon.

At 2.5 wt% D-AlNiCo particle addition, as shown in Fig. 4a, it can be observed that the white θ-phase has a block-like form in α-Al matrix, while the γ-phase has a skeleton-like form, as arrowed in Fig. 4e. However, when the addition level of D-AlNiCo particles exceeds 5.0 wt% (Fig. 4b–d), the θ-phase content increases in the composites, and the distribution of the particles is quite regular. As shown in Fig. 4f–h, the θ-phase mainly exhibits a blocky-shape, with its size ranging from 15 to ~40 μm, while the γ-phase is distributed in the interdendritic regions and has a fine skeleton-shape or blocky-shape. From the microstructural observations, it was also found that the sizes of the θ-phase and γ-phase particles are much smaller than that of the original D-AlNiCo particles.

According to the Al–Ni–Co ternary phase diagram [20], the decagonal quasicrystalline phase cannot coexist with the Al phase. So, diffusion should occur when the $Al_{72}Ni_{12}Co_{16}$ particles are introduced into the Al melt. From the above microstructural analysis (Fig. 4), the white particles in the composites are quaternary intermetallic compounds. These observations indicate that when the D-AlNiCo particles are introduced into the Al melt, serious compositional diffusion occurs between the D-AlNiCo particles and the Al melt via heat, mass, and momentum transport [3]. During the liquid fabrication processing of Al-base composites reinforced by a quasicrystal phase, the diffusion between the Al matrix and the quasicrystal phase is inevitable, and the thermodynamic stability of the quasicrystal phase depends on the temperature and time. When the Al-base composites are prepared by solid state vacuum sintering at 525 °C, the structure of the quasicrystal can be sustained and just a thin diffusion layer at the interface between the Al matrix and quasicrystal phase [9]. However, higher heating temperature (≥400 °C) leads to the disappearance of the quasicrystal and formation of ternary crystalline Al_7Cu_2Fe phase in the Al-base composites [12, 13, 21]. During hot pressing, as the temperature increases from 600 to 700 °C, a series of phase transformations occurs in the $(Al_{65}Cu_{20}Cr_{15})_p$/Al composites, and the structure of the quasicrystalline particles finally transforms into the equilibrium phase Θ [10]. In our study, during the stirring process, dissolution of the sharp outer edges of the D-AlNiCo quasicrystalline particles occurs first, and a diffusion layer forms between the inner regions of the particles and the Al melt. Then the reaction proceeds through the whole quasicrystalline particle, resulting in the disappearance of the quasicrystal particles and the formation of the new crystalline phases. The continuous intensive stirring accelerates the dissolution and fragmentation of the particles. The above information indicated that, when the Al-base composites are fabricated by mechanical stirring method, the diffusion reaction between the quasicrystal phase and the Al melt is too rapid to control, and the structure of the quasicrystal is completely changed. Cheng et al. [22] proved that the reaction was completed within 20 s in the Al/$Al_{72}Ni_{12}Co_{16}$ system. The addition of D-AlNiCo particles changes the local temperature field and concentration field around the particles, which favors the nucleation and growth of newly

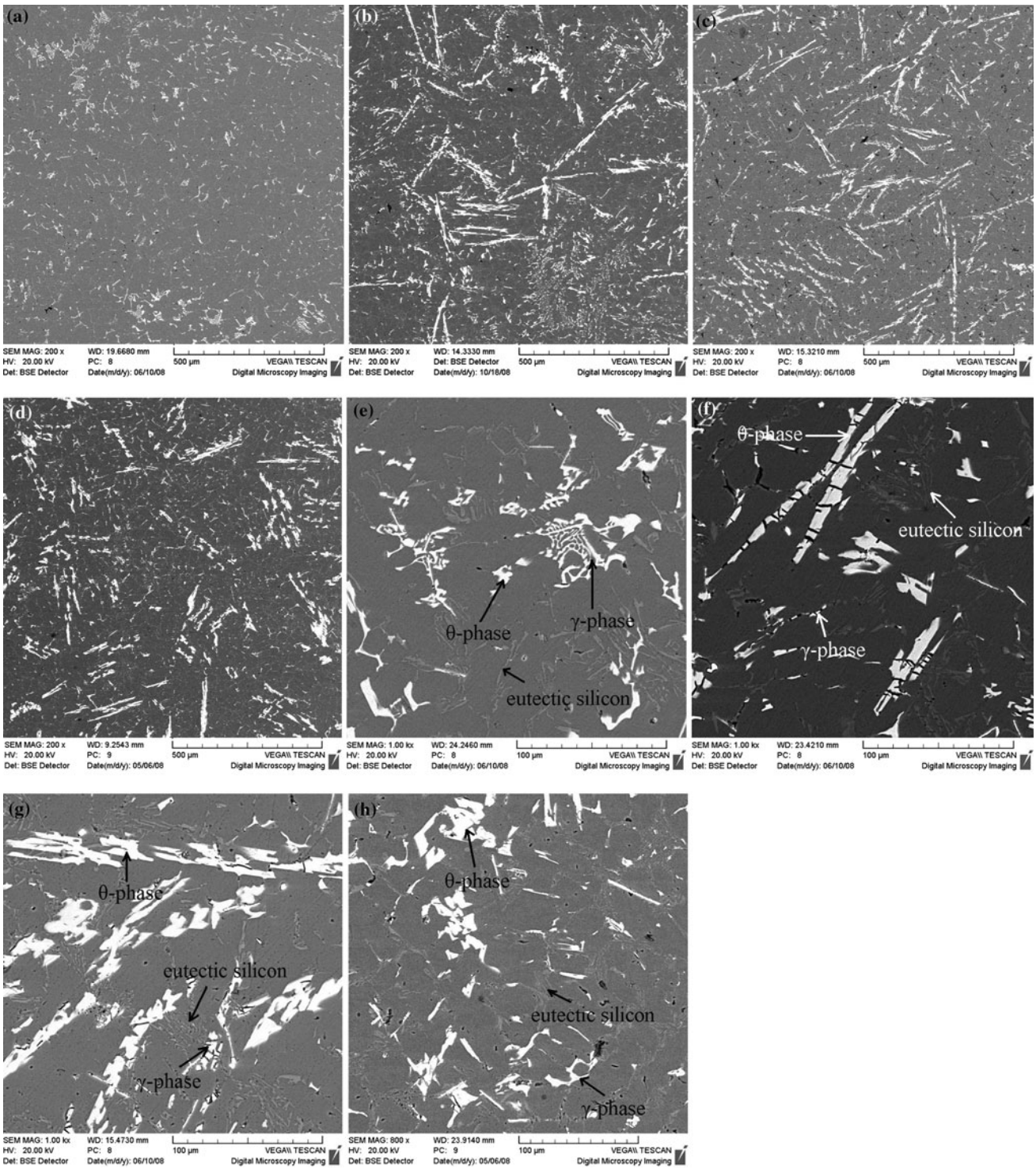

Fig. 4 BSE images showing the microstructures of the as-cast A356Al-based composites with x wt% $Al_{72}Ni_{12}Co_{16}$ quasicrystalline particles. **a**, **e** $x = 2.5$; **b**, **f** $x = 5.0$; **c**, **g** $x = 7.5$; **d**, **h** $x = 10$

formed crystalline phases. Thus, two phases with different compositions are obtained in α-Al matrix and interdendritic regions, respectively. When equilibrium is reached, the compositions of θ-phase and γ-phase remain stable.

Mechanical properties

The hardness and tensile properties of the A356Al-base composites were determined. Table 2 shows the tensile

Table 1 Chemical compositions of the two white intermetallic compounds identified by EDS analysis in the as-cast composites (Range in at.%)

Element	Al Kα	Si Kα	Ni Kα	Co Kα
θ-phase	69.75–84.05	1.21–1.93	3.98–6.16	9.41–14.03
γ-phase	77.07–86.81	0.80–3.84	8.65–16.03	0.71–4.37

Table 2 Mechanical properties of the as-cast A356Al-base composites

Particle content (wt%)	σ_b (MPa)	$\sigma_{0.2}$ (MPa)	δ (%)	HB
0	164.09	92.73	4.03	57.9
2.5	172.50	102.50	3.88	70.2
5.0	170.00	108.75	3.63	72.4
7.5	155.00	110.00	3.17	72.4
10.0	147.75	115.25	2.55	69.7

strength (σ_b), yield strength ($\sigma_{0.2}$), elongation percentage (δ%), and Brinell hardness (HB) of the as-cast A356Al-base composites. It can be seen that σ_b increases at first, reaches a maximum value of 172.50 MPa for a 2.5 wt% D-AlNiCo particle addition, then decreases until it reaches a value below that of the A356 base alloy with increasing addition of D-AlNiCo particles. As the addition of D-AlNiCo particles increases, $\sigma_{0.2}$ increases steadily. From Table 2, it is found that the value of δ equals to 4.03%. However, after introducing D-AlNiCo particles, the δ of the as-cast A356Al-base composites was decreased remarkably into 3.88–2.55%.

Microhardness measurements showed that the presence of AlCuFe quasicrystalline particles considerably increase the microhardness of the matrix in the as-cast Al-base composites by conventional casting method [23]. As shown in Table 2, the Brinell hardness of the A356 base alloy is 57.9. After adding D-AlNiCo particles, the Brinell hardness of the A356Al-base composites is greatly improved. Compared to the A356 base alloy, the improvement in Brinell hardness of the composites was about 20–25%, ascribed to the dispersion of reinforcing particles in the composite matrix.

Strengthening mechanisms

During the past two decades, the strengthening mechanisms of composites have been extensively documented [2, 3, 24–27]. From Table 2, the values of $\sigma_{0.2}$ in the A356Al-base composites are improved by about 10.5–24% as compared to that of the A356 base alloy. As identified by EDS, small amount of the dissolution of Ni, and Si elements in α-Al matrix results in the solid solution strengthening of the composites. Although the Al–Ni–Co decagonal quasicrystals are not sustained as the reinforcement particles, the resulting crystalline phases, θ-phase and γ-phase, can still act as effective reinforcements for promoting the tensile strength of the composites.

It has been proved that the dislocation density in the composite matrix is higher than that in the unreinforced matrix [28, 29]. The dislocation density ρ caused by the large difference between the coefficients of thermal expansion (CTE) of the reinforcing particles and Al matrix can be expressed as:

$$\rho = \frac{12\Delta T \Delta C f_p}{bd} \quad (1)$$

where, ΔT and ΔC are the temperature difference and thermal expansion coefficient difference between the reinforcement particles and Al matrix, respectively, f_p is the volume fraction of the particles, b is the Burger's vector, and d is the particle size.

Thermal residual stress due to thermal expansion dislocation strengthening has a direct effect on the yield strength of PRMMCs. The incremental increase in yield strength $\Delta\sigma_{CTE}$ of the composites due to thermal expansion dislocation strengthening can be estimated as:

$$\Delta\sigma_{CTE} = \alpha G b \rho^{1/2} \quad (2)$$

with G is the shear modulus of the matrix, α a parameter showing the dislocation strengthening efficiency. As the crystalline phases in the composites, θ-phase and γ-phase, are the final reaction products, the detailed thermodynamic parameters could not be given in the present study. During cooling, the differences of CTE between Al matrix and the reinforcing particles result in sufficient stress to cause plastic deformation. Thus, dislocations could be generated in order to accommodate the heterogeneous plastic flow in the vicinity of the deforming matrix [28]. When a misfit strain $\varepsilon \approx 1\%$ is developed in the Al/SiC_p system, a dislocation density, $\rho = 1.8\times10^{13}$ m^{-2}, is generated as calculated from the calculation through $\varepsilon = \rho L b$ [3]. The intensity of dislocation generation at the interface between the Al matrix and the reinforcing particles is associated with the shape and size of the latter. From their investigation of the relationship between particle size and the plastic zone, Lee et al. [30] pointed out that the degree of plastic relaxation is strongly dependent on particle size, and the plastic zone size increases with increasing particle size. Thus, dislocation generation increases significantly with the increase of particle size, and higher deformed regions result in higher dislocation density, and vice versa.

Although the tensile strength of the as-cast A356Al-base composites can be improved, there exists a major limitation with respect to ductility. As shown in Table 2, the higher the fraction of the reinforcing particles, the lower the ductility. Figure 5 shows the fracture surface of a tensile-

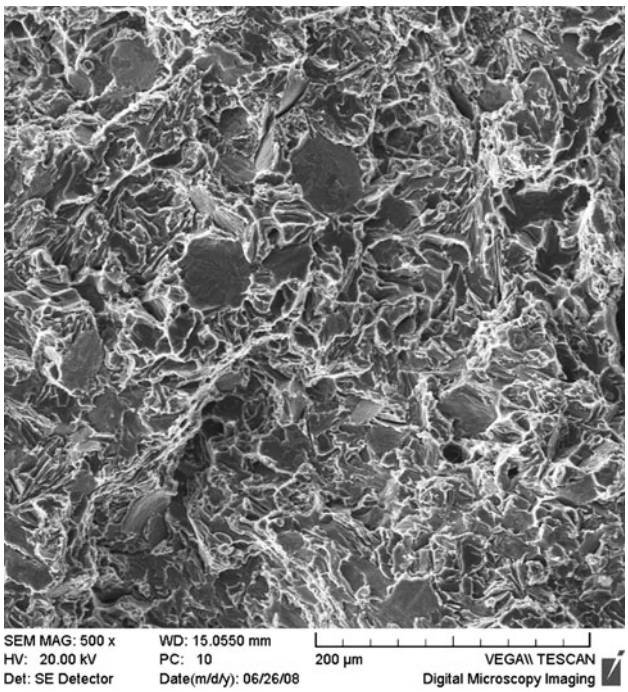

Fig. 5 Fracture surfaces of the as-cast A356Al-base composites containing 2.5 wt% $Al_{72}Ni_{12}Co_{16}$ quasicrystalline particles

tested sample of as-cast A356Al-base composite reinforced with 2.5 wt% D-AlNiCo particles. The fracture surface of the composite displays typical brittle fracture mode. There is very little plastic deformation before failure occurs. Due to the inherent brittleness of the reinforcement and eutectic silicon, brittle cleavage is observed across the reinforcing particles and eutectic silicon.

The damage of A356 can proceed following three events: particle cracking, microcrack formation and growth, and local linkage of microcracks [31]. According to the deformation and fracture processes, cracking of the eutectic silicon and reinforcing particles is an important factor influencing the ductility. As the α-Al matrix in the composites is quite soft, it undergoes certain plastic deformation. The deformation of the reinforcing particles and eutectic silicon remains elastic due to much higher yield stress. Thus, the stress concentration within the particles would be very high. When a load is applied, the matrix responds for most of the load, after which the load is transferred to the reinforcing particles. For the present composites, the reinforcing particles, i.e., the θ-phase and γ-phase particles, are the brittle constituents, and they tend to generate microcracks even at low strain [32, 33], due to the low fracture strength required to initiate microcracks. The coarser and larger reinforcing particles have a higher probability of initiating defects, and tend to fracture first under the applied stress. It has been demonstrated that larger size and higher volume fraction of the SiC_p in Al/SiC_p composites result in lower ductility [2–4, 34]. The increase in the volume fraction will increase the volume fraction of the microcracks initiated. Additionally, the non-uniform distribution of the reinforcing particles (Fig. 4) will increase the size of the microcracks and decrease the length of the ligament locally. So, the ductility of the composites is therefore reduced.

Conclusions

(1) Serious compositional diffusion occurs between $Al_{72}Ni_{12}Co_{16}$ quasicrystalline particles and the Al melt. When the reaction is completed, two crystalline phases, θ-phase and γ-phase, are formed in the as-cast AlA356-Al–Ni–Co composites. SEM observations show that the Co-rich θ-phase distributes in the α-Al matrix, while Ni-rich γ-phase together with eutectic silicon forms in the interdendritic regions. Microstructure observations show that eutectic silicon remains coarse flake-like or acicular in shape in the composites, and EDS results reveal that no Ni or Co elements are detected in the eutectic silicon.

(2) The final reaction products, θ-phase and γ-phase, serve as reinforcing particles to influence the mechanical properties. As the addition level of D-AlNiCo particles increases, the yield strength of the as-cast A356Al-base composites is improved, while the ductility is reduced correspondingly. Also, the Brinell hardness of the as-cast composites is greatly improved by 20–25% compared to the base A356 alloy.

(3) The strengthening mechanism of the composites could be mainly associated with (a) solid solution strengthening in α-Al matrix, (b) differences of coefficients thermal expansion between the Al matrix and the reinforcing particles. In addition, the occurrence of θ-phase within the α-Al matrix improves the interfacial bonding between the θ-phase and α-Al matrix, which, in turn, improves the tensile properties of the as-cast composites. The fracture surfaces of the as-cast A356Al-base composites indicate that they exhibit typical brittle fracture mode.

Acknowledgements The authors thank the National Natural Science Foundation of China for financial support (Grant.50571081). The authors would also express their thanks to J.J. Li and Z. Chen of the State Key Laboratory of Solidification Processing.

References

1. Mortensen A, Jin I (1992) Int Mater Rev 37:101
2. Lloyd DJ (1994) Int Mater Rev 39:1
3. Ibrahim IA, Mohamed FA, Lavernia EJ (1991) J Mater Sci 26:1137. doi:10.1007/BF00544448

4. Samuel AM, Liu H, Samuel FH (1993) J Mater Sci 28:6785. doi: 10.1007/BF00356432
5. Ünlü BS (2008) Mater Des 29:2002
6. Shechtman D, Blech I, Gratias D (1984) Phys Rev Lett 53:1951
7. Tsai AP, Aoki K, Inoue A (1993) J Mater Res 8:5
8. Tang F, Anderson IE, Biner SB (2003) Mater Sci Eng A 363:20
9. Tang F, Anderson IE, Biner SB (2002) J Light Metals 2:201
10. Qi YH, Zhang ZP, Hei ZK (1999) J Alloy Compd 285:221
11. Eckert J, Schurack F, Schultz L (2003) J Metast Nanocryst Mater 15–16:245
12. Tcherdyntsev VV, Kaloshkin SD, Shelekhov EV (2004) J Metast Nanocryst Mater 20–21:157
13. Kaloshkin SD, Tcherdyntsev VV, Laptev AI (2004) J Mater Sci 39:5399. doi:10.1023/B:JMSC.0000039253.28721.3f
14. Yokoyama Y, Note R, Kimura S (1997) Mater Trans JIM 38:943
15. Fisher IR, Kramer MJ, Islam Z (1999) Philos Mag B 79:425
16. Gräber M, Barz RU, Dreier P (2000) Mater Sci Eng A 294–296:143
17. Liu XB (2003) PhD Thesis, Northwestern Polytechnical University (in Chinese)
18. Bokhonov B, Korchagin M (2004) J Alloy Compd 368:152
19. Yu JQ (1987) Illustrated handbook of binary phase diagrams. Shanghai Scientific and Technical Press, p 134 and 149 (in Chinese)
20. Gödecke T, Scheffer M, Lück R (1998) Z fur Metall 89:270
21. Köster U, Liu W, Liebertz H (1993) J Non-Cryst Solids 153/154: 446
22. Cheng SL, Yang GC, Wang JC (2009) J Mater Sci 44:3420. doi: 10.1007/s10853-009-3454-3
23. Fleury E, Lee SM, Chio G (2001) J Mater Sci 36:963. doi: 10.1023/A:1004875824039
24. McDaniels DL (1985) Metall Trans A 16:1105
25. Nardone VC, Prewo KM (1986) Scr Metall 20:43
26. Arsenault RJ, Shi N (1986) Mater Sci Eng A 81:175
27. Arsenault RJ, Wang L, Feng CR (1991) Acta Metall Mater 39:47
28. Uogelsang M, Arsenault RJ, Fisher RM (1986) Metall Mater Trans A 17:379
29. Arsenault RJ, Shi N, Feng CR (1991) Mater Sci Eng A 131:55
30. Lee JK, Earmme YY, Aaronson HI (1980) Metall Trans A 11: 1837
31. Wang QG (2003) Metall Mater Trans A 34:2887
32. Hahn GT, Rosenfield AR (1975) Metall Trans A 6:653
33. Thompson DS (1975) Metall Trans A 6:671
34. Song M, Huang DW (2009) Metall Mater Trans A 38:2127